those of the grid at the event of both the grid connection and islanding to reduce any voltage changes across the critical loads. Since this scheme is independent of the load characteristics, it can be applicable for any current and voltage controllers. Further development of the indirect current control strategy has been reported in [11] and [12]. In these works, the indirect current controller is always operated in voltage control mode to prevent voltage transients in the event of grid failure. Even though the aforementioned control methods can ensure the stability of load voltages under the intentional mode transitions, they did not take the unintentional islanding into account. To provide seamless mode transition to grid connected-inverters at both the intentional and unintentional islanding, several control approaches have been presented [13], [14]. However, since the grid voltage distortions have not been taken into account in the aforementioned control methods, the quality of the injected currents are relatively poor under abnormal grid conditions.

To address this issue, this paper proposes an enhanced multiloop control scheme for an LCL-filtered grid-connected inverter which is mainly based on a proportional integral resonant (PI+RES) controller. By using the proposed control scheme, the quality of injected currents can be guaranteed regardless of the grid voltage conditions with a relatively simple control structure. In addition to theoretical analysis, the comparative simulation results are provided to confirm the effectiveness of the proposed control scheme.

SYSTEM MODELING

Fig. 1 shows the schematic of a three-phase grid-connected inverter connected to the grid through LCL filters. In this configuration, the inverter is in charge of not only injecting the power into the grid but also supplying power to critical local loads. The inverter system can be mathematically expressed in *abc*-frame as

$$v^{abc} - v_{cf}^{abc} = R_1 i_1^{abc} + L_1 \frac{di_1^{abc}}{dt} \tag{1}$$

$$i_1^{abc} - i_2^{abc} = C_f \frac{dv_{cf}^{abc}}{dt} \tag{2}$$

$$v_{cf}^{abc} - e^{abc} = R_2 i_2^{abc} + L_2 \frac{di_2^{abc}}{dt} \tag{3}$$

where v, v_{cf}, and e denote the inverter voltage, capacitor voltage, and grid voltage, respectively, i_1 and i_2 denote the inverter-side current and grid-side current, respectively, R_1, R_2, L_1, L_2, and C_f denote the resistances, inductances, and capacitance of the filters, respectively.

The system equations in (1)-(3) can be transformed into the synchronous reference frame (SRF) as

$$v^{qd} - v_{cf}^{qd} = R_1 i_1^{qd} + L_1 \frac{di_1^{qd}}{dt} \pm L_1 \omega i_1^{dq} \tag{4}$$

$$i_1^{qd} - i_2^{qd} = C_f \frac{dv_{cf}^{qd}}{dt} \pm C_f \omega v_{cf}^{dq} \tag{5}$$

$$v_{cf}^{qd} - e^{qd} = R_2 i_2^{qd} + L_2 \frac{di_2^{qd}}{dt} \pm L_2 \omega i_2^{dq} \tag{6}$$

where ω denotes the angular frequency of the grid voltage.

Since the coupling terms in (4)-(6) merely influence the dynamics of the overall system, they are omitted in the controller design process for convenience. Then, the transfer functions of the inverter system can be derived from (4)-(6) as

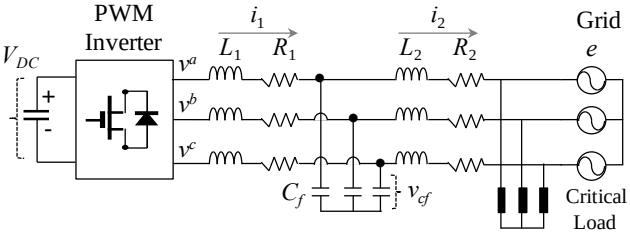

Figure 1: Schematic of a Three-phase Grid-connected Inverter System

$$G_1(s) = \frac{I_1^{qd}(s)}{V^{qd}(s) - V_{cf}^{qd}(s)} = \frac{1}{L_1 s + R_1} \tag{7}$$

$$G_c(s) = \frac{V_{cf}^{qd}(s)}{I_1^{qd}(s) - I_2^{qd}(s)} = \frac{1}{C_f s} \tag{8}$$

$$G_2(s) = \frac{I_2^{qd}(s)}{V_{cf}^{qd}(s) - E^{qd}(s)} = \frac{1}{L_2 s + R_2}. \tag{9}$$

To further facilitate the design and analysis of the proposed control system, the open-loop transfer function of the inverter system can be obtained from (7)-(9) as

$$G_{op}(s) = \frac{G_1(s)G_2(s)G_c(s)}{1 + G_1(s)G_c(s) + G_2(s)G_c(s)} = \frac{1}{as^3 + bs^2 + cs + d} \tag{10}$$

where $a = C_f L_1 L_2$, $b = C_f(L_1 R_2 + L_2 R_1)$, $c = L_1 + L_2 + C_f R_1 R_2$, and $d = R_1 + R_2$.

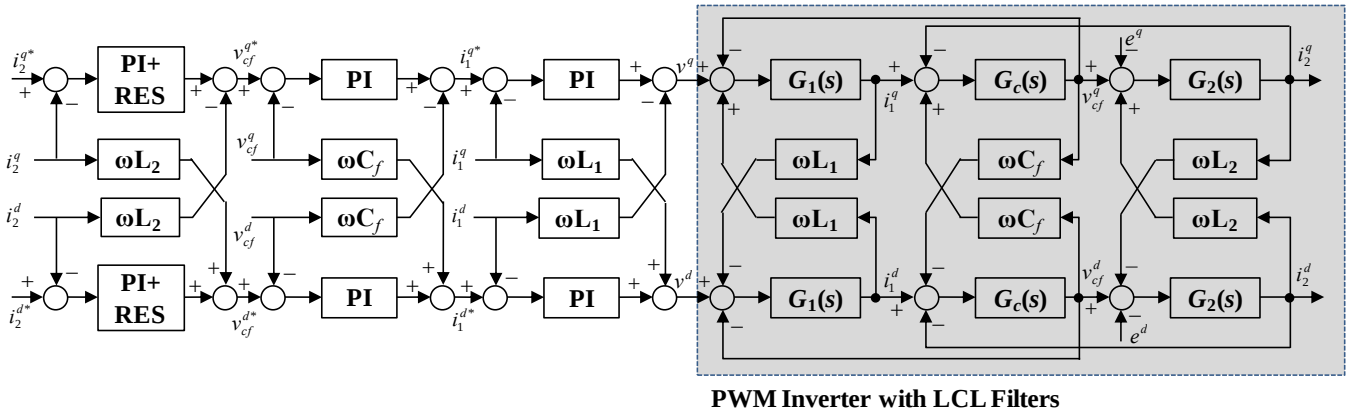

Figure 2: Overall Block Diagram of the Proposed Enhanced Multiloop Control Scheme

Proposed Enhanced Multiloop Control Scheme

To ensure the stability of the inverter output voltage in the event of operation mode transition, the proposed control scheme consists of three control loops, namely, inverter-side current control loop, capacitor voltage control loop, and grid-side-current control loop. An individual controller is implemented for each of these control loops. Since the inverter operates as a voltage source in the islanded mode, the grid-side current control loop is inactive in this mode. Therefore, only the capacitor voltage controller and inverter-side current controller are used in the islanded mode. Since the grid voltage is excluded from this mode, the conventional PI controllers are sufficient to control the inverter. The transfer function of a conventional PI controller can be expressed as

$$G_{PI}(s) = \frac{K_p s + K_I}{s} \tag{11}$$

where K_P and K_I are the proportional and integral gains, respectively.

From (7) and (11), the closed-loop transfer function of the inverter-side current control loop can be given as

$$G_{cl1}(s) = \frac{G_1(s)}{1 + G_{PI1}(s)G_1(s)} = \frac{s}{L_1 s^2 + (K_{P1} + R_1) + K_{i1}} \tag{12}$$

where K_{P1} and K_{I1} are the proportional and integral gains of the inverter-side current controller, respectively.

Similarly, the closed-loop transfer function of the capacitor voltage control loop can be derived from (8) and (11) as

$$G_{clc}(s) = \frac{G_c(s)}{1 + G_{PIc}(s)G_c(s)} = \frac{s}{C_f s^2 + K_{Pc} s + K_{ic}} \tag{13}$$

where K_{Pc} and K_{Ic} are the proportional and integral gains of the capacitor voltage controller, respectively.

In addition to tracking the constant reference values, the grid-side current controller should be able to reject the sinusoidal disturbances caused by the grid voltage distortions. In order to accomplish this requirement, the distorted grid voltages need to be taken into consideration in designing the grid-side current controller. In general, the grid voltage is composed of a fundamental term and harmonic terms. In the SRF, the fundamental grid voltages become constant values which can be easily rejected by using the conventional PI controller. As opposed to the fundamental term, the harmonic-polluted components of the grid voltage still vary sinusoidally with time in the SRF. To deal with these sinusoidal disturbances, resonant terms are added to the conventional PI controller to form a PI+RES controller. The resonant terms can be expressed as

$$G_{RES}(s) = \frac{2K_{RESi}\omega_{ci} s}{s^2 + 2\omega_{ci} + \omega_i^2} \tag{14}$$

where $i = 6k \pm 1$ denotes the order of the harmonics with k being positive integers, K_{RES} is the resonant gain, ω_{ci} is the cut-off frequency, and ω is the resonant frequency.

From (11) and (14), the PI+RES controller for the grid-side current control loop can be expressed as

$$G_{PI+RES}(s) = K_{P2} + \frac{K_{I2}}{s} + \frac{2K_{RES6}\omega_{c6} s}{s^2 + 2\omega_{c6} + \omega_6^2} + \frac{2K_{RES12}\omega_{c12} s}{s^2 + 2\omega_{c12} + \omega_{12}^2}. \tag{15}$$

It is worth noticing that the controller in (15) is synthesized by considering that the grid voltage consists of the fundamental term and the harmonic terms in the orders of the 5th, 7th, 11th, and 13th. By means of the Park's transformation, these harmonic disturbances are transformed into the harmonics in the orders of the 6th and 12th in the SRF.

Form (9) and (15), the closed-loop transfer function of the grid-side current controller can be derived as

$$G_{clc}(s) = \frac{G_c(s)}{1 + G_{PI+RES}(s)G_c(s)} \tag{16}$$

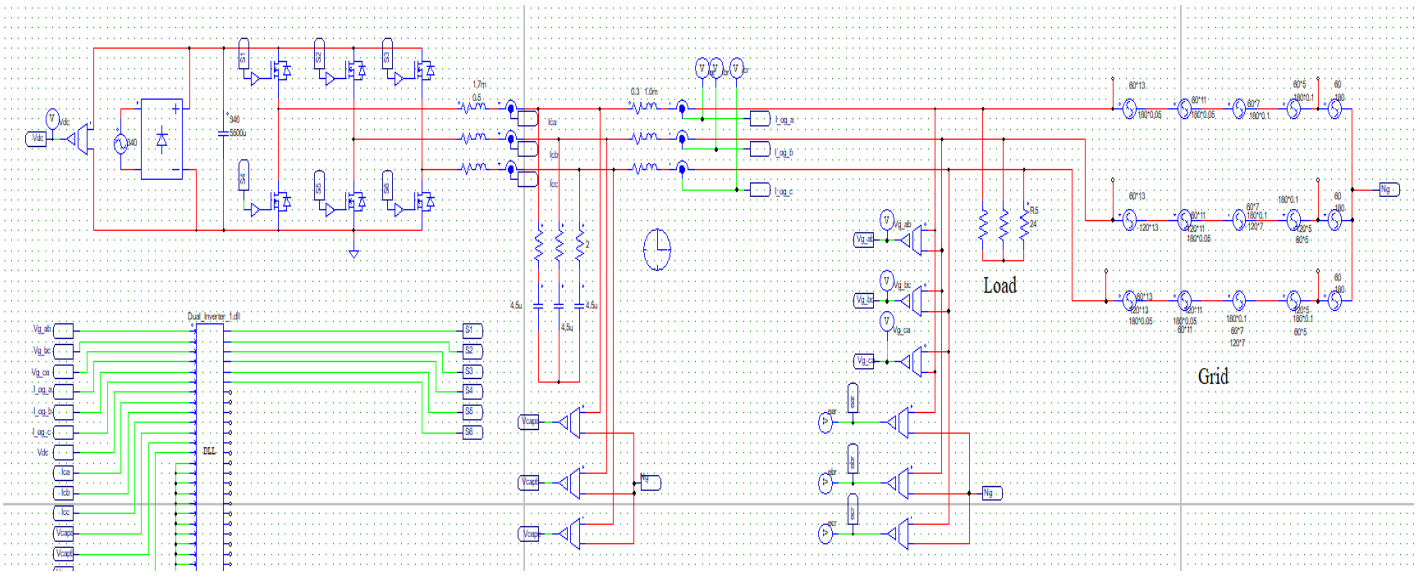

Figure 3: Simulation Configuration for a Grid-connected Inverter System

From the closed-loop transfer functions in (12), (13), and (16), the control gains can be calculated such that the stability of the overall system is guaranteed. By choosing a proper set of gains, other criteria such as the transient and steady-state requirements can be easily fulfilled. The entire block diagram of the proposed enhanced multiloop control scheme as well as the detailed inverter model is shown in Fig. 2. To further improve the control performance, the coupling terms are included as feed-forward terms in the proposed control scheme as shown in Fig. 2.

SIMULATION RESULTS

To validate the effectiveness of the proposed control scheme, the simulations have been carried out using the PSIM software. The simulation model for an LCL-filtered grid-connected inverter is constructed as shown in Fig. 3. The main controllers are implemented using the PSIM DLL block.

To verify the robustness of the proposed control scheme against the abnormal grid environment, the harmonically distorted grid voltages are considered in addition to the ideal grid voltages. The distorted grid voltages are formed by adding 10% of the 5^{th} and 7^{th} harmonics with respect to the nominal voltage, and 5% of the 11^{th} and 13^{th} harmonics with respect to the nominal voltage into the ideal grid voltage. For performance comparison, the conventional indirect current control scheme is used to highlight the superior performance of the proposed control scheme. The conventional indirect current controller consists of three control loops based on the PI controllers as reported in [13].Fig. 4 shows the simulation results of the conventional indirect current control scheme under the ideal grid voltages. As can be observed from Fig. 4(b), the conventional indirect current controller provides reasonably sinusoidal steady-state current waveforms. Moreover, Fig. 4(c) and Fig. 4(e) shows considerably fast transient current responses under a step change in the reference current.

Fig. 5 shows the simulation results of the conventional indirect current control scheme under distorted grid voltages as given in Fig. 5(a). As opposed to the results in Fig. 4(b), the steady-state responses of grid-side currents are severely distorted due to adverse grid voltages as shown in Fig. 5(b). The harmful distortions can also be observed in the Fig. 5(c), Fig. 5(d), and Fig. 5(e).

To highlight the effectiveness of the proposed control scheme, Fig. 6 shows the simulation results of the proposed enhanced multiloop control scheme. As can be clearly seen from Fig. 6(b), the grid-side three-phase currents remain quite sinusoidal regardless of highly distorted grid voltage. Moreover, Fig. 6(c) and Fig 6(e) reveal that the proposed control scheme still provides fast and stable transient responses. It is worth mentioning that the inverter-side currents and capacitor voltages are distorted due to the distorted grid voltage. However, these distortions do not influence the grid-side currents. Therefore, the results in Fig. 6 confirm that the proposed control scheme can provide better control performance than that of the conventional indirect current control scheme.

Fig. 7 shows the FFT results of *a*-phase current for two control schemes under different grid conditions. As can be observed from Fig. 7(a) and Fig. 7(b), the inability of the conventional indirect current control scheme to deal with sinusoidal disturbances leads to considerably high THD level of injected current. On the contrary, as shown in Fig. 7(c), the proposed control scheme well retains the THD level of the injected current even under heavily distorted grid voltages.

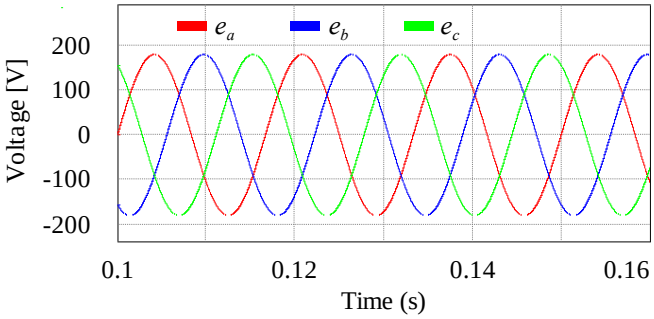

(a) Three-phase grid voltages

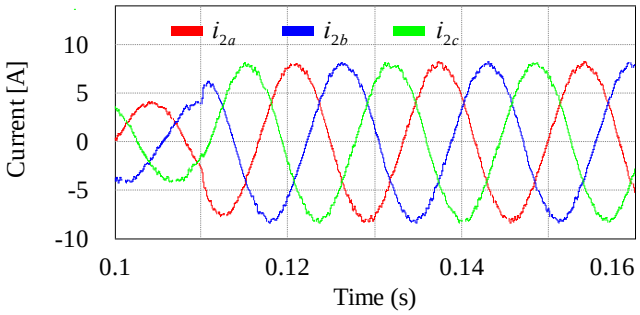

(b) Three-phase grid-side currents

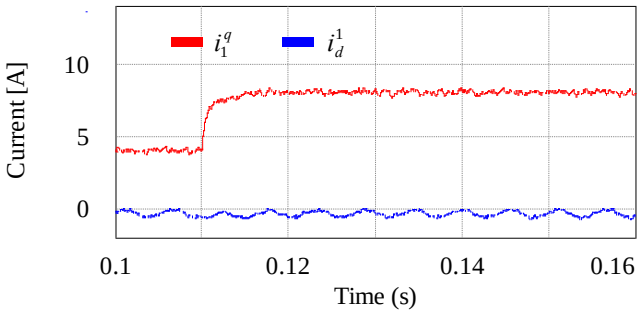

(c) Inverter-side currents in the SRF

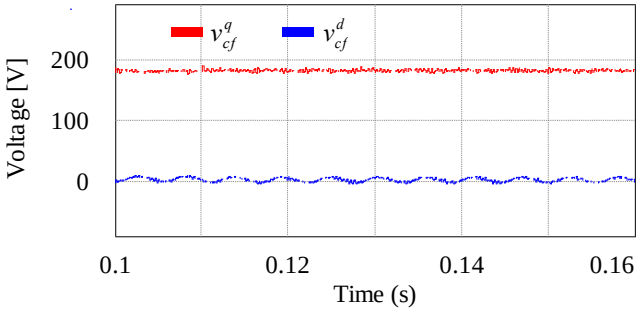

(d) Capacitor voltages in the SRF

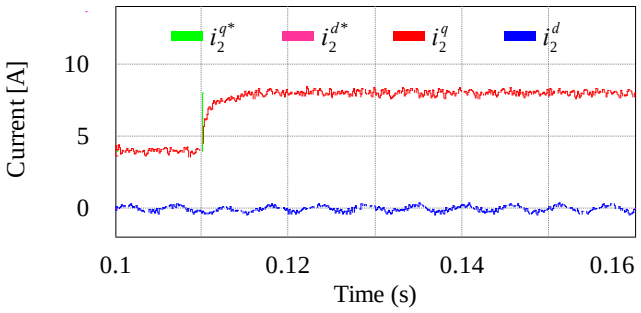

(e) References and grid-side currents in the SRF

Figure 4: Simulation Results of the Conventional Indirect Current Control Scheme under the Ideal Grid Voltage

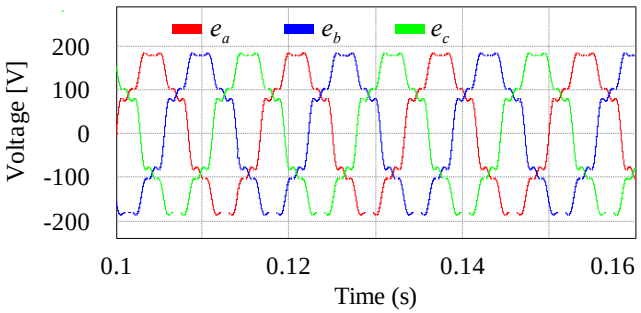

(a) Three-phase grid voltages

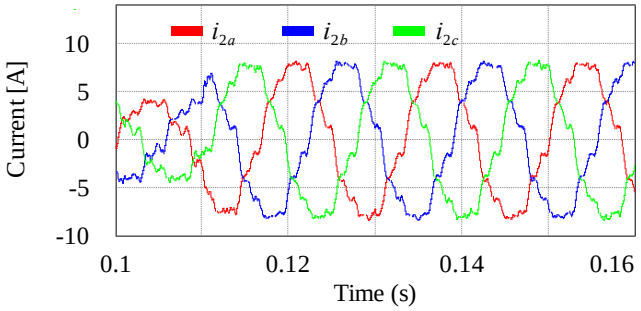

(b) Three-phase grid-side currents

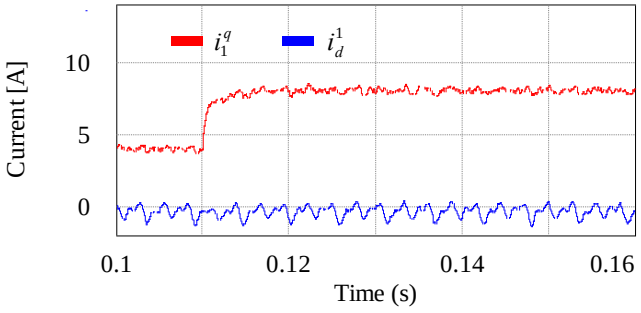

(c) Inverter-side currents in the SRF

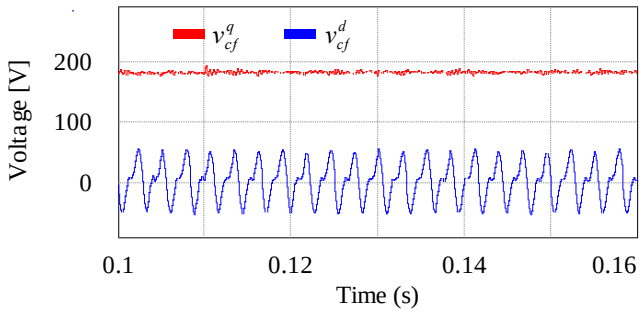

(d) Capacitor voltages in the SRF

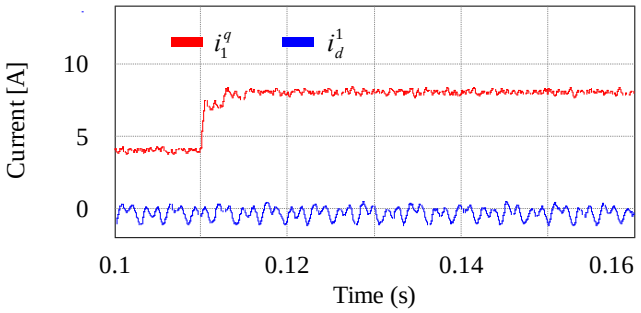

(c) Inverter-side currents in the SRF

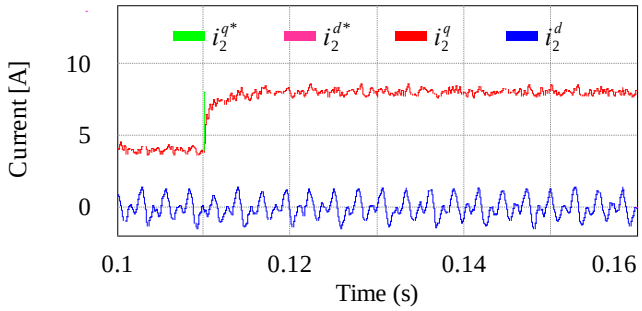

(e) References and grid-side currents in the SRF

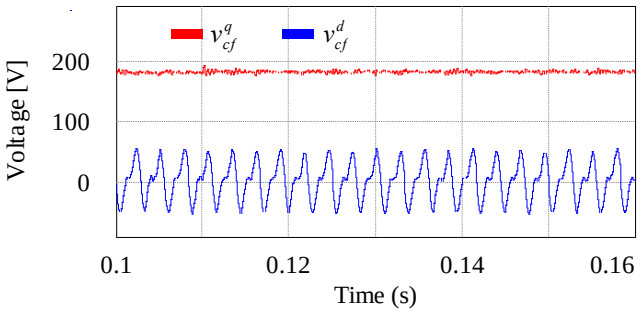

(d) Capacitor voltages in the SRF

Figure 5: Simulation Results of the Conventional Indirect Current Control Scheme under Distorted Grid Voltages

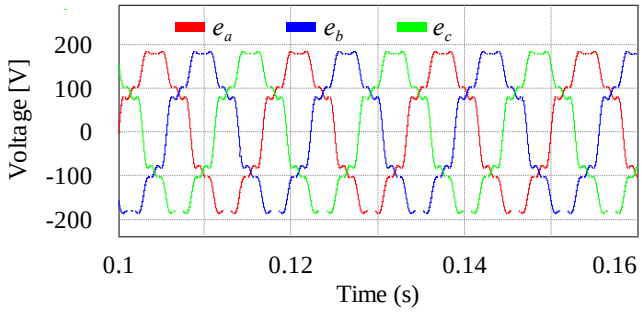

(a) Three-phase grid voltages

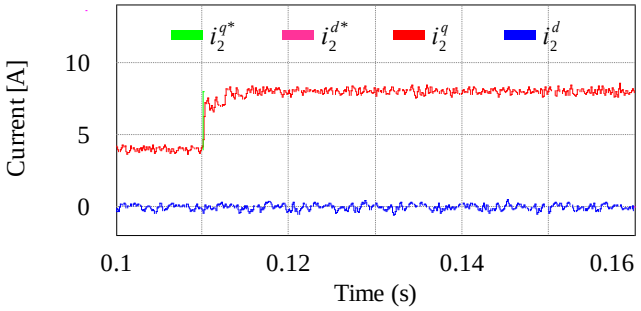

(e) References and grid-side currents in the SRF

Figure 6: Simulation Results of the Proposed Control Scheme under Distorted Grid Voltages

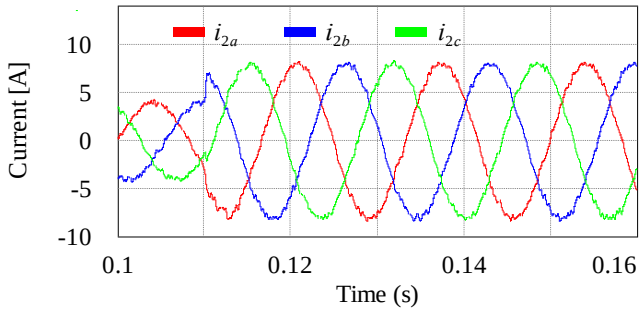

(b) Three-phase grid-side currents

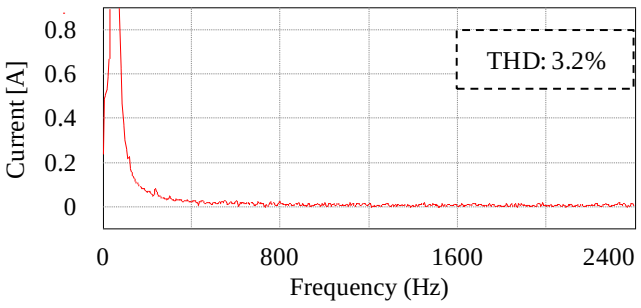

(a) Conventional indirect current control scheme under the ideal grid voltages

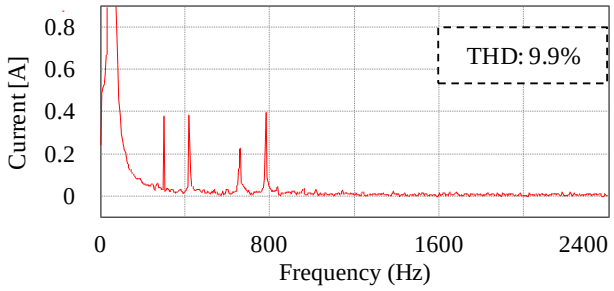

(b) Conventional indirect current control scheme under distorted grid voltages

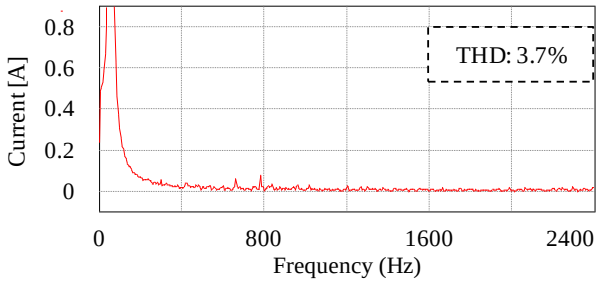

(c) Proposed control scheme under distorted grid voltages

Figure 7: FFT Results of Grid-side a-phase Current

CONCLUSION

An effective control of a grid-connected inverter under the transition of operation mode is one of the key issues in microgrid operation. Conventionally, the multiloop and indirect current control schemes have been used to cope with the unexpected transient voltages supplied to critical loads. However, the adverse grid conditions have not been taken into consideration in these control strategies, which leads to poor quality of the injected currents when the grid voltages are distorted. To address this problem, this paper presents an enhanced multiloop control scheme for a three-phase inverter connected to the grid through LCL filters. The proposed control scheme is composed of a PI+RES controller and two PI controllers in cascade. While the PI controllers are used in both the inverter-side current control loop and capacitor voltage control loop, the PI+RES controller is employed in the grid-side current control loop. As a result of using the PI+RES controller, the quality of injected currents is significantly improved even under severely distorted grid voltages. Theoretical analyses and comparative simulation results have been provided to confirm the usefulness of the proposed control scheme.

ACKNOWLEDGEMENTS

This study was supported by the Research Program funded by the SeoulTech (Seoul National University of Science and Technology).

REFERENCES

[1] M. J. Jang and K. H. Kim, “Cooperative and autonomous control strategy of AC microgrid with energy storage system,” SERSC Int. Jour. of Control and Aut., vol. 10, no. 5, pp. 47-64, May 2017.

[2] J. de Matos, F. e Silva, and L. Ribeiro, “Power control in AC isolated microgrids with renewable energy sources and energy storage systems,” IEEE Trans. Ind. Electron., vol. 62, no. 6, pp. 3490–3498, Jun. 2014.

[3] T. H. Nguyen and K. H. Kim, “Finite control set-model predictive control with modulation to mitigate harmonic component in output current for a grid-connected inverter under distorted grid conditions,” Energies, vol. 10, no. 7, pp. 1–25, Jul. 2017.

[4] H. Han, X. Hou, J. Yang, J. Wu, M. Su, and J. M. Guerrero, “Review of power sharing control strategies for islanding operation of AC microgrids,” IEEE Trans. Smart Grid, vol. 7, no. 1, pp. 200–215, Jan. 2016.

[5] J. M. Guerrero, J. C. Vasquez, J. Matas, L. G. de Vicuna, and M. Castilla, “Hierarchical control of droop-controlled AC and DC microgrids—a general approach toward standardization,” IEEE Trans. Ind. Electron., vol. 58, no. 1, pp. 158–172, Jan. 2011.

[6] IEEE Std. 1547-2003. Standard for interconnecting distributed resources with electric power systems. IEEE. 2003.

[7] IEC 61727 Ed.2. Photovoltaic (PV) systems – characteristic of the utility interface. IEC. 2003.

[8] O. C. Montero-Hernández and P. N. Enjeti, “Ride-through for critical loads,” IEEE Ind. Appl. Mag., vol. 8, no. 6, pp. 45–53, Dec. 2002.

[9] O. C. Montero-Hernández and P. N. Enjeti, “Ride-through for critical loads,” IEEE Ind. Appl. Mag., vol. 8, no. 6, pp. 45–53, Dec. 2002.

[10] R. Tirumala, N. Mohan, and C. Henze, “Seamless transfer of grid-connected PWM inverters between utility-interactive and stand-alone modes,” APEC. Seventeenth Annu. IEEE Appl. Power Electron. Conf. Expo. (Cat. No.02CH37335), vol. 2, no. c, pp. 1081–1086, Mar. 2002.

[11] H. Kim, T. Yu, and S. Choi, “Indirect current control algorithm for utility interactive inverters in distributed generation systems,” IEEE Trans. Power Electron., vol. 23, no. 3, pp. 1342–1347, May 2008.

[12] Z. Yao, L. Xiao, and Y. Yan, “Seamless transfer of single-phase grid interactive inverters between grid-connected and stand-alone modes,” IEEE Trans. Power Electron., vol. 25, no. 6, pp. 1597-1603, Jun. 2010.

[13] Y. Prabowo and S. Choi, “Improved indirect current

control for utility-interactive inverter system with critical load," vol. 2, no. 1, pp. 1–5, Nov. 2016.

[14] S. Yoon, H. Oh, S. Choi, "Controller design and implementation of indirect current control based utility-interactive inverter system," IEEE Trans. Power Electron., vol. 28, no. 1, Jan. 2013.